

## Temperature dependence of the surface free energy and surface stress: An atomistic calculation for Cu(110)

T. Frolov\* and Y. Mishin†

Department of Physics and Astronomy, George Mason University, MSN 3F3, Fairfax, Virginia 22030, USA  
(Received 7 November 2008; published 30 January 2009)

We propose a method to deduce the free energies  $\gamma$  and stresses  $\tau$  of plane surfaces and solid-liquid interfaces in elemental systems from atomistic simulations involving nonhydrostatically stressed solid phases. The method is applied to compute the temperature dependencies of  $\gamma$  and  $\tau$  for the (110) Cu surface using Monte Carlo simulations with an embedded-atom potential. Both quantities decrease with temperature but remain different even near the bulk melting point despite extensive premelting of this surface. This difference is explained by the existence in the premelted surface structure of a solid-liquid interface with relatively small but finite values of  $\gamma$  and  $\tau$ . Separate calculations of the (110) solid-liquid interface stress give a negative value, suggesting that this interface is in a state of compression. This study motivates future work on anisotropy of surface/interface free energies and stresses, and on the extension of this method to more complex systems.

DOI: 10.1103/PhysRevB.79.045430

PACS number(s): 68.08.-p, 65.40.-b, 68.03.Cd

### I. INTRODUCTION

The surface free energy  $\gamma$  and the surface stress  $\tau_{ij}$  are fundamental quantities in surface thermodynamics. Gibbs<sup>1</sup> defined the surface free energy as reversible work per unit area needed to create a new surface and the surface stress as reversible work of elastically stretching the surface. These two quantities are related by<sup>2</sup>

$$\tau_{ij} = \delta_{ij}\gamma + \frac{\partial\gamma}{\partial e_{ij}}, \quad i, j = 1, 2, \quad (1)$$

where the derivative is taken at a constant temperature,  $e_{ij}$  is a strain tensor of the surface, and  $\delta_{ij}$  is the Kronecker symbol. Two of the Cartesian axes are assumed to be parallel to the surface and the third one is normal to it. While  $\gamma$  is a scalar, the surface stress  $\hat{\tau}$  is a symmetrical second-rank tensor. These quantities are usually of the same order of magnitude. Due to the second term in Eq. (1), components of  $\hat{\tau}$  can be larger than  $\gamma$ , smaller, or even negative, which  $\gamma$  can never be.<sup>1</sup> Defining the average surface stress as  $\tau = (\tau_{11} + \tau_{22})/2$ , Eq. (1) can be rewritten as

$$\tau = \gamma + A \frac{\partial\gamma}{\partial A}, \quad (2)$$

where  $A$  is the surface area.

The fundamental differences between  $\gamma$  and  $\hat{\tau}$  have been recently discussed by Kramer and Weissmüller.<sup>3</sup> In contrast to solids,  $\gamma$  and  $\tau$  of liquids are numerically equal because liquids respond to strains by exposing more or less atoms to the surface without changing  $\gamma$ , resulting in  $\partial\gamma/\partial e_{ij} = 0$ .<sup>3-5</sup> At high temperatures,  $\gamma$  of a solid can exceed the sum of the liquid-vacuum and solid-liquid free energies. To minimize the free energy, the solid surface can premelt, creating a thin liquidlike layer.<sup>6</sup> Gurney<sup>7</sup> argued that because at high temperatures surface atoms can migrate like in a liquid, the surface free energy should become equal to the surface stress. This assumption was later used in the experimental work of Bailey and Watkins.<sup>8</sup> Herring<sup>9</sup> disagreed with Gurney's con-

clusion, questioning the way Gurney related the chemical potentials of the surface atoms to the surface stress.

Unfortunately, most of the data for surface stresses reported in the literature refer to either 0 K or to a certain fixed temperature, making it difficult to determine whether  $\tau$  and  $\gamma$  converge with temperature. The temperature dependence of  $\gamma$  was studied experimentally<sup>10</sup> and by atomistic simulations,<sup>11,12</sup> and it was found that  $\gamma$  decreases with temperature. The experiments of Vermaak and Wilsdorf<sup>10</sup> indicated that the second term in Eq. (1) linearly increased with temperature.

Equation (1) can also be applied to solid-liquid interfaces provided that the derivative is taken along a constant-temperature direction on the solid-liquid coexistence surface in the parameter space. It can be expected that  $\tau$  and  $\gamma$  will be again different, but this has not been tested experimentally. Recent atomistic simulations indicate that  $\tau$  of solid-liquid interfaces can be positive or negative depending on the material.<sup>13</sup>

The goal of this work is to clarify the behavior of the surface stress and surface free energy with temperature, particularly near the bulk melting point. We employ atomistic computer simulations using a (110) copper surface as a model. For the interpretation of the surface premelting behavior, we have also studied isolated solid-liquid and liquid-vacuum interfaces. Our calculations of the surface and interface properties are based on thermodynamics relations that we derive here in a mathematical form suitable for atomistic calculations.

Such derivations are needed for the following reasons. Taking surface stress as an example, Eq. (1) can be rewritten as

$$\tau_{ij} = \frac{\partial(\gamma A)}{A \partial e_{ij}}, \quad i, j = 1, 2, \quad (3)$$

where  $\gamma A$  is the total excess free energy of a surface whose area  $A$  can vary only by elastic straining without changing the number of surface atoms. This equation can be simplified by using Lagrangian coordinates, i.e., coordinates attached to

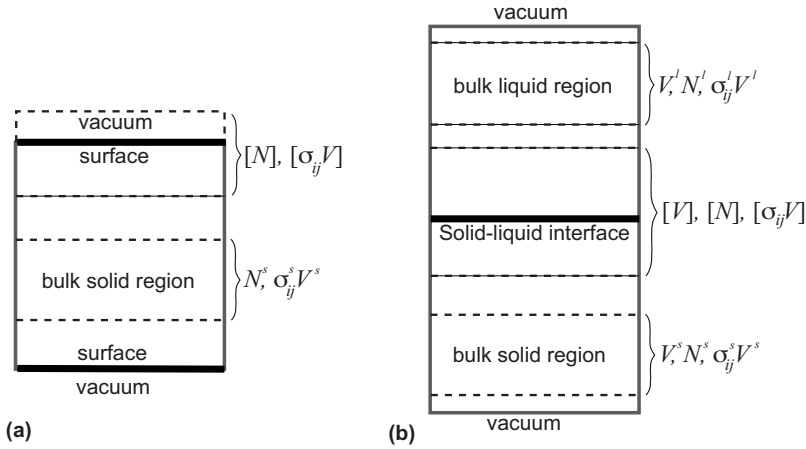


FIG. 1. Simulation blocks and positions of the interface and bulk regions employed in the calculations of thermodynamic properties of (a) solid surfaces and (b) solid-liquid interfaces. The quantities computed in different regions are indicated. The bracketed quantities refer to the surface/interface layer, whose bounds can be chosen arbitrary as long as they lie within the homogeneous bulk phases. The bulk regions can lie beyond the surface/interface layer, as in this figure, or inside it (not shown).

the crystal lattice.<sup>1,4,14</sup> In the Lagrangian formulation, a certain state of the solid is chosen as a reference and all other states are considered as derived from it by appropriate elastic deformations. The strain tensor,  $e_{ij}^L$ , is then taken with respect to the reference state, the surface free energy  $\gamma^L$  is taken per unit reference area, and the surface and bulk stresses ( $\tau_{ij}^L$  and  $\sigma_{ij}^L$ ) are defined as forces per unit reference length/area. Using the Lagrangian quantities, some thermodynamic equations can be rewritten in a more compact form than in terms of real physical quantities. For example, the Lagrangian surface stress becomes simply  $\tau_{ij}^L = \partial \gamma^L / \partial e_{ij}^L$  instead of Eq. (3).<sup>4,14</sup>

Despite certain advantages, using Lagrangian quantities is not convenient for atomistic calculations. Such calculations give immediate access to instantaneous physical quantities, such as the system dimensions, energy, and stress. Because the cross-sectional area of the simulation block usually contains a fixed number of unit cells of the solid, all properties of the surface or interface *automatically* correspond to the same Lagrangian state. Thus, there is no need to specify a particular reference state and introduce the respective Lagrangian quantities. As will be shown in this paper, it is easier to formulate computational recipes and perform the calculations in terms of directly accessible physical parameters.

In Sec. II and Appendix we show how surface excess quantities, particularly  $\hat{\tau}$  and  $\gamma$ , can be extracted from raw simulation data. After introducing our methodology (Sec. III), we perform atomistic simulations of thermodynamics of the (110) Cu surface at temperatures from 0 K to the bulk melting point (Sec. IV). In Sec. IV we compute the stresses of the solid-liquid and liquid-vacuum interfaces. In Sec. V we analyze our results and draw conclusions.

## II. THERMODYNAMIC RELATIONS

In this section we derive the relations of surface thermodynamics that will be used in this work. Although we are interested in the surface/interface free energy  $\gamma$ , it is convenient to formulate all equations in terms of the *total* excess free energy of the simulation block,  $\gamma A$ , and defer a separation of  $\gamma$  until the end of the calculation. In all thermodynamic processes considered here,  $A$  changes by elastic defor-

mation only, so that the Lagrangian area of the surface/interface remains constant. Although in the atomistic simulations presented later in this paper the solid is almost stress free, it still contains some residual stresses which are not hydrostatic. To enable corrections for such residual stresses, all equations will be derived for the general case of a nonhydrostatically stressed solid. The cases of a solid surface and a solid-liquid interface will be discussed separately.

### A. Solid surface

Consider an elemental solid in a nonhydrostatic state of strain whose plane surface is exposed to vacuum. It can be shown (see the Appendix) that reversible variations in the total excess free energy are given by

$$d(\gamma A) = -[S/X]dT - [N/X]df^s + \sum_{i,j=1,2} [\sigma_{ij}V/X]de_{ij}, \quad (4)$$

where the state variables are temperature  $T$ , the Helmholtz free energy per atom of the bulk solid  $f^s$ , and the elastic strain tensor  $\hat{e}$ . Conjugate to these variables are the surface excesses of the entropy  $S$ , of the number of atoms  $N$ , and of the volume-averaged lateral components of the stress tensor  $\hat{\sigma}$  multiplied by the total volume  $V$ . As  $\gamma A$ , these excess quantities refer to the *entire* simulation block not per unit surface area. To satisfy mechanical equilibrium, one of the principal axes of  $\hat{\sigma}$  must be normal to the surface with  $\sigma_{33} = 0$ . Following the method of Cahn,<sup>4</sup> we have expressed the surface excesses through the determinants in which, for example,

$$[S/X] \equiv \frac{\begin{vmatrix} [S] & [X] \\ S^s & X^s \end{vmatrix}}{X^s} = [S] - S^s[X]/X^s,$$

with similar expressions for the excesses of  $N$  and  $\sigma_{ij}V$ . Here  $X$  is one of the extensive quantities  $S$ ,  $N$ , or  $\sigma_{ij}V$ , which can be chosen arbitrarily. The square brackets, such as  $[S]$  or  $[X]$ , indicate the amount of the extensive quantity in a thick enough layer containing the surface [Fig. 1(a)]. One of the bounds of the layer is placed in vacuum and the other in the bulk of the solid, both far enough from the surface to neglect its effect. The superscript  $s$  refers to properties of a homogeneous solid region chosen as a comparison system. Since

$[X/X]=0$ , one of the terms in Eq. (4) is necessarily zero, reflecting the constraint imposed by the bulk equation of state. It can be shown that the remaining terms express  $d(\gamma A)$  as a perfect differential and that the surface excesses do not depend on the thickness of the surface layer as long as its bounds are beyond the influence of the surface.<sup>4</sup>

Choosing  $X=N$ , Eq. (4) becomes

$$\begin{aligned} d(\gamma A) &= -[S/N]dT + \sum_{i,j=1,2} [\sigma_{ij}V/N]de_{ij} \\ &\equiv -S^{\text{ex}}dT + \sum_{i,j=1,2} \tau_{ij}Ade_{ij}, \end{aligned} \quad (5)$$

where  $\tau_{ij}$  is the surface-stress tensor given by

$$\begin{aligned} \tau_{ij} &= \frac{1}{A} \left( \frac{\partial(\gamma A)}{\partial e_{ij}} \right)_T \\ &= \frac{[\sigma_{ij}V/N]}{A} \\ &= \frac{\begin{vmatrix} [\sigma_{ij}V] & [N] \\ \sigma_{ij}^s V^s & N^s \end{vmatrix}}{AN^s} = \frac{[\sigma_{ij}V] - \sigma_{ij}^s V^s [N]/N^s}{A} \end{aligned} \quad (6)$$

[we used Eq. (3)], and  $S^{\text{ex}}$  is the excess entropy,

$$S^{\text{ex}} \equiv [S/N] = [S] - S^s[N]/N^s. \quad (7)$$

Furthermore, with this choice of  $X$ ,  $\gamma A$  itself becomes the excess of the Helmholtz free energy:  $\gamma A = [F/N]$  (see the Appendix). Therefore,

$$\gamma A = [U - TS/N] = U^{\text{ex}} - TS^{\text{ex}}, \quad (8)$$

where

$$U^{\text{ex}} = [U/N] = [U] - U^s[N]/N^s \quad (9)$$

is the total excess of internal energy. Combining Eqs. (5) and (8), we obtain

$$d\left(\frac{\gamma A}{T}\right) = -\frac{U^{\text{ex}}}{T^2}dT + \frac{1}{T} \sum_{i,j=1,2} \tau_{ij}Ade_{ij}. \quad (10)$$

This equation can be used for computations of  $\gamma A$  by thermodynamic integration. For example, consider a process in which temperature is increased while the solid is stretched biaxially to maintain zero bulk stress,  $\sigma_{ij}^s=0$  ( $i, j=1, 2, 3$ ), at every temperature. In this process, the biaxial strain  $e$  increases with temperature to accommodate the thermal expansion of the solid. As a result,  $T$  and  $e$  are no longer independent variables and Eq. (10) becomes

$$d\left(\frac{\gamma A}{T}\right) = -\frac{U^{\text{ex}}}{T^2}dT + \frac{2\tau A}{T} \left(\frac{\partial e}{\partial T}\right)_{\sigma_{ij}^s=0} dT. \quad (11)$$

The second term in the right-hand side includes the linear thermal-expansion factor,

$$\alpha = \frac{1}{a} \left( \frac{\partial a}{\partial T} \right)_{\sigma_{ij}^s=0} = \left( \frac{\partial e}{\partial T} \right)_{\sigma_{ij}^s=0}, \quad (12)$$

where  $a$  is the bulk lattice parameter of the solid at temperature  $T$ . Note that  $\alpha$  is a function of temperature only, same as  $U^{\text{ex}}$ ,  $A$ , and  $\tau$ . Knowing  $(\gamma A)_0$  at some reference temperature  $T_0$ , Eq. (11) can be integrated to obtain  $\gamma A$  at another temperature  $T$ ,

$$\gamma A(T) = (\gamma A)_0 \frac{T}{T_0} + T \int_{T_0}^T \left[ -\frac{U^{\text{ex}}}{T'^2} + \frac{2\alpha\tau A}{T'} \right] dT'. \quad (13)$$

In atomistic simulations,  $U^{\text{ex}}$ ,  $\tau$ , and  $\alpha$  can be computed for a set of temperatures and used to obtain  $\gamma A(T)$  by numerical integration of Eq. (13). The physical value of  $\gamma$  is then recovered by dividing  $\gamma A$  by the physical area of the surface at the respective temperature. This procedure was implemented in this work as will be discussed later.

## B. Solid-liquid interface

Consider the same nonhydrostatically stressed solid but now in contact and equilibrium with its melt at a pressure  $p$ . The mechanical equilibrium condition between the two phases requires that one of the principal axes of the stress tensor in the solid be normal to the interface with  $\sigma_{33}=-p$ . The differential of total excess free energy of the solid-liquid interface is given by (see the Appendix)

$$\begin{aligned} d(\gamma A) &= -[S/XY]dT + [V/XY]dp - [N/XY]d\mu \\ &+ \sum_{i,j=1,2} [(\sigma_{ij} + \delta_{ij}p)V/XY]de_{ij}, \end{aligned} \quad (14)$$

where  $\mu$  is the chemical potential in the liquid. Any two of the intensive variables  $S$ ,  $V$ ,  $N$ , or  $(\sigma_{ij} + \delta_{ij}p)V$  (denoted by  $X$  and  $Y$ ) can be eliminated because each phase imposes a constraint expressed by a Gibbs-Duhem equation.<sup>4</sup> The determinant  $[Z/XY]$  is defined by

$$[Z/XY] = \frac{\begin{vmatrix} [Z] & [X] & [Y] \\ Z^s & X^s & Y^s \\ Z^l & X^l & Y^l \end{vmatrix}}{\begin{vmatrix} X^s & Y^s \\ X^l & Y^l \end{vmatrix}}. \quad (15)$$

As before, the square brackets designate the extensive property  $Z$  of a thick enough layer containing the interface [Fig. 1(b)], whereas the superscripts  $s$  and  $l$  refer to arbitrarily chosen regions of the homogeneous solid and liquid phases. It can be shown that this determinant gives the total excess of the extensive property  $Z$  over the bulk phases under conserved values of the extensive properties  $X$  and  $Y$ .<sup>4</sup>

Choosing  $N$  and  $V$  for  $X$  and  $Y$ , Eq. (14) reduces to

$$d(\gamma A) = -S^{\text{ex}}dT + \sum_{i,j=1,2} \tau_{ij}Ade_{ij}, \quad (16)$$

with the interface stress tensor given by

$$\tau_{ij} = \frac{[(\sigma_{ij} + \delta_{ij}p)V/NV]}{A} = \frac{\begin{vmatrix} [(\sigma_{ij} + \delta_{ij}p)V] & [N] & [V] \\ (\sigma_{ij}^s + \delta_{ij}p)V^s & N^s & V^s \\ 0 & N^l & V^l \end{vmatrix}}{A \begin{vmatrix} N^s & V^s \\ N^l & V^l \end{vmatrix}}. \quad (17)$$

The excess entropy  $S^{\text{ex}} = [S/NV]$  is given by a similar expression.

Equations (6) and (17) express the surface and interface stresses  $\tau_{ij}$  as excesses of the stress tensor  $\hat{\sigma}$  in forms convenient for computations. They involve only extensive properties and do not require calculations of interface profiles. For the particular case of a hydrostatic solid or a liquid system, these equations reduce to

$$\tau_{ij} = [\sigma_{ij}V]/A \quad (\text{plane solid or liquid surface}), \quad (18)$$

$$\tau_{ij} = [(\sigma_{ij} + \delta_{ij}p)V]/A \quad (\text{plane solid-liquid interface}). \quad (19)$$

Equations (6) and (17) will be used in the atomistic simulations discussed in the rest of the paper.

### III. METHODOLOGY OF ATOMISTIC SIMULATIONS

#### A. Simulated models

We chose copper as a model material with atomic interactions described with an embedded-atom method (EAM) potential fit to experimental and first-principles data.<sup>15</sup> This potential accurately reproduces the lattice parameter, cohesive energy, elastic constants, phonon frequencies, thermal expansion, lattice-defect energies, and other properties of Cu. The melting temperature of Cu predicted by this potential is  $T_m = 1327$  K (1356 K in experiment).

The (110) surface was modeled in a  $26 \times 25 \times 41 \text{ \AA}^3$  (2240 atoms) simulation block with periodic boundaries in the  $x$  and  $y$  directions and free surfaces in the  $z$  direction, a geometry which mimics an infinitely large thin film [Fig. 2(a)]. The coordinate axes were aligned parallel to  $[\bar{1}10]$ ,  $[001]$ , and  $[110]$ , respectively. To study a liquid surface, the film was completely melted by increasing the temperature above  $T_m$  and cooled down to temperatures of interest around  $T_m$ .

The (110) solid-liquid interface was modeled in a  $26 \times 25 \times 110 \text{ \AA}^3$  (5600 atoms) block containing a  $\sim 40\text{-\AA}$ -thick solid layer sandwiched between two  $\sim 35 \text{ \AA}$  thick liquid layers exposed to vacuum [Fig. 2(b)]. The solid part had the same crystallographic orientation as the previously described solid film with periodic boundary conditions in  $x$  and  $y$ . The exposure to vacuum guaranteed zero pressure in the liquid.

Prior to the MC simulations, each block was uniformly expanded by the linear thermal-expansion factor at the simulated temperature using the expansion factors computed previously.<sup>15</sup> Although this pre-expansion eliminated most of the thermal stresses in the solid, there were always some

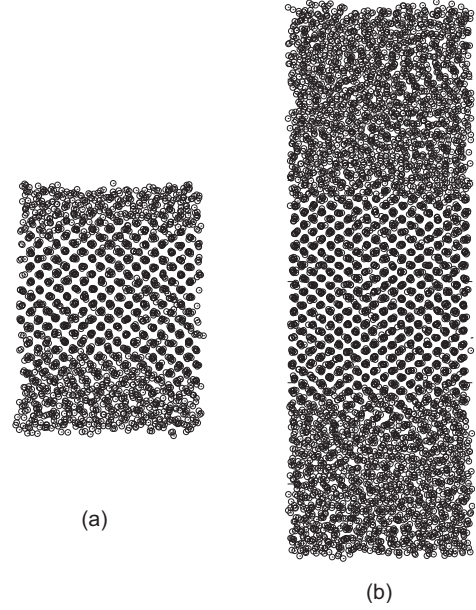


FIG. 2. Typical Monte Carlo (MC) snapshot of (a) (110) solid film at 1320 K and (b) (110) solid-liquid coexistence system at 1327 K. The open circles mark instantaneous atomic positions projected on the  $(1\bar{1}0)$  plane parallel to the page. The top and bottom surfaces of both systems are exposed to vacuum. The distances  $h$ ,  $d$ , and  $d'$  are discussed in text.

nonhydrostatic residual stresses due to statistical errors in the thermal-expansion factors.

#### B. Monte Carlo simulations

Off-lattice MC simulations<sup>16,17</sup> were employed to study the surface and interface properties at finite temperatures. Although the same calculations could have been implemented with molecular dynamics, we wanted to use the same method as in our ongoing work on binary Cu-based alloys. In alloys, the formation of an equilibrium surface/interface segregation requires a redistribution of the chemical species over the system by diffusion mechanisms, which makes molecular-dynamics simulations highly impractical.

In the MC simulations, the system volume and temperature are fixed while the atoms are movable. At each MC step, a randomly chosen atom is displaced by a random amount in a random direction and this move is accepted or rejected by the Metropolis algorithm. At each temperature, the initial configuration was brought to equilibrium by  $10^4$ – $10^5$  MC steps per atom (depending on the system size), followed by a production run of  $(2\text{--}6) \times 10^5$  additional MC steps. Snapshot files containing instantaneous atomic positions were saved every 20–30 MC steps and used in subsequent calculations of stresses, energies, and other properties.

The solid surface calculations were performed at temperatures from 0 to 1320 K, the liquid surface calculations at 1300, 1327, and 1350 K, and the solid-liquid interface calculation at 1327 K only. In the latter case, despite spontaneous random displacements of the interfaces during the simulations, the solid layer thickness remained at least 35  $\text{\AA}$  and

the thickness of each liquid layers at least 25 Å. These thicknesses were considered large enough to neglect interactions between the interfaces.

### C. Structural order analysis

To analyze the structural changes in the surface region and to identify the interface positions, we employed the structure factor  $S(\mathbf{k})$ , whose modulus is given by

$$|S(\mathbf{k})| = \frac{1}{N} \sqrt{\left[ \sum_i \cos(\mathbf{k}\mathbf{r}_i) \right]^2 + \left[ \sum_i \sin(\mathbf{k}\mathbf{r}_i) \right]^2}, \quad (20)$$

where  $\mathbf{k} = 2\pi[2\sqrt{2}/a, 0, 0]$  is a chosen reciprocal-lattice vector parallel to the  $x$  direction,  $\mathbf{r}_i$  is the radius vector of atom  $i$ , and the summation goes over the  $N$  atoms contained in a region of interest.  $|S(\mathbf{k})|$  is equal to 1 for perfectly ordered fcc structure at 0 K and 0 for a disordered structure such as liquid. The structure factor was computed for a set of layers parallel to the surface/interface and plotted as a function of distance  $z$  normal to the layers.

For the solid surface, positions of (220) atomic planes in the bulk were identified and extrapolated toward the surface, keeping the total number of real and extrapolated planes constant at all temperatures. Each atom was assigned to the nearest plane and  $|S(\mathbf{k})|$  was computed by summation over the atoms assigned to each plane. At low temperatures, the  $|S(\mathbf{k})|$  values thus obtained refer to actual atomic planes. When the surface becomes disordered at high temperatures, the  $|S(\mathbf{k})|$  values in the surface region are formally assigned to imaginary planes, whereas the values in the bulk still refer to the actual atomic planes. The average structure factor,  $|S(\mathbf{k})|_{\text{top}}$ , of the top two surface layers was used as a metric of surface disorder. The thickness  $h$  of the surface region was estimated as the distance between the top surface plane and the point at which  $|S(\mathbf{k})|(z) \approx [|S(\mathbf{k})|_{\text{top}} + |S(\mathbf{k})|_s]/2$ , where  $|S(\mathbf{k})|_s$  is the value of the structure factor in the bulk solid.

For the block containing two solid-liquid interfaces,  $|S(\mathbf{k})|$  was computed for atoms located within 6-Å-thick windows parallel to the interfaces. The profile  $|S(\mathbf{k})|(z)$  was calculated by moving the center of the window by small increments in the  $z$  direction. The interface positions were estimated from the relation  $|S(\mathbf{k})|(z) \approx |S(\mathbf{k})|_s/2$ . The liquid surface positions were identified with the maximum and minimum values of the  $z$  coordinates of all atoms.

The interface positions defined through the structure factor slightly depend on the choice of the  $\mathbf{k}$  vector. There is also some arbitrariness in the positions of the liquid surfaces. We emphasize, however, that we do not assign to these definitions of the surface/interface positions any thermodynamic meaning. We use them only as a guide for selecting reasonable bounds of the homogeneous bulk regions as discussed below.

### D. Surface and interface stress calculations

EAM permits direct calculations of the average stress tensor  $\sigma_{ij}$  of a system using the virial expression<sup>18</sup>

$$\sigma_{ij}V = \left[ \sum_{\substack{(\alpha,\beta) \\ \alpha \neq \beta}} \left\{ \left[ \frac{1}{2} \Phi'(r_{\alpha\beta}) + \Psi'(\bar{\rho}_\alpha) \rho'(r_{\alpha\beta}) \right] \frac{r_{\alpha\beta}^i r_{\alpha\beta}^j}{r_{\alpha\beta}} \right\} - Nk_B T \delta_{ij} \right], \quad (21)$$

where the symbols  $\alpha$  and  $\beta$  enumerate atoms,  $i$  and  $j$  are Cartesian components of the vectors and tensors,  $r_{\alpha\beta}^i$  is the vector connecting atoms  $\alpha$  and  $\beta$  separated by a distance  $r_{\alpha\beta}$ ,  $\Phi(r_{\alpha\beta})$  is the pair interaction function,  $\rho(r_{\alpha\beta})$  is the electron-density function assigned to atoms,  $\Psi(\bar{\rho}_\alpha)$  is the embedding energy of atom  $\alpha$ ,  $\bar{\rho}_\alpha$  is the host electron density on atom  $\alpha$ ,  $V$  is the volume of the system,  $k_B$  is the Boltzmann constant, and the prime indicates differentiation of the functions.

The surface and interface stresses were computed from Eqs. (6), (18), and (17) for each individual snapshot, and the results were averaged over all snapshots. Note that those equations contain only products of the stresses times the respective volumes, which are given directly by the right-hand side of Eq. (21). Thus, the calculation does not require partitioning of the volume between atoms. For the solid and liquid surfaces, the quantities  $[\sigma_{ij}V]$  and  $[N]$  were computed for the entire simulation block. For the solid surface, the bulk values of  $\sigma_{ij}^s V^s$  and  $N^s$  were calculated for an inner region of the film, whose bounds were a distance  $d$  away from the upper and lower surfaces.

For the solid-liquid interface,  $[\sigma_{ij}V]$ ,  $[V]$ , and  $[N]$  were determined for a layer whose bounds were a distance  $d$  away from the upper and lower liquid surfaces and which contained two solid-liquid interfaces. A region inside the solid layer that was separated by a distance  $d'$  from each of the solid-liquid interfaces was selected to compute  $\sigma_{ij}^s V^s$ ,  $V^s$ , and  $N^s$ . Similarly,  $V^l$  and  $N^l$  were computed for bulk liquid regions chosen a distance  $d'$  always from the solid-liquid interfaces and a distance  $d$  away from the liquid surfaces.

The distances  $d$  and  $d'$  were chosen to be large enough to exclude the influence of the surfaces and interfaces on bulk quantities, which was verified by increasing these distances until the computed surface/interface stresses reached constant values within statistical errors of the calculations. Typical values of  $d$  and  $d'$  were around 9 Å. Note that these distances were taken relative to the *instantaneous* positions of the interfaces in each snapshot. Since the interfaces constantly deviated slightly away from their average positions due to thermal fluctuations, the bulk regions selected for the stress calculations varied from one snapshot to another, implementing additional statistical averaging of the bulk properties.

In addition to averaging over the snapshots, the final values of the surface/interface stresses were obtained by averaging over several different choices of  $d$  and  $d'$ . The error bars of the calculations were estimated by dividing the entire set of  $3 \times 10^4$  snapshots into ten subsets and computing the standard deviation of the subset averages from the global average. Clearly, this error bar depends on the number of subsets.

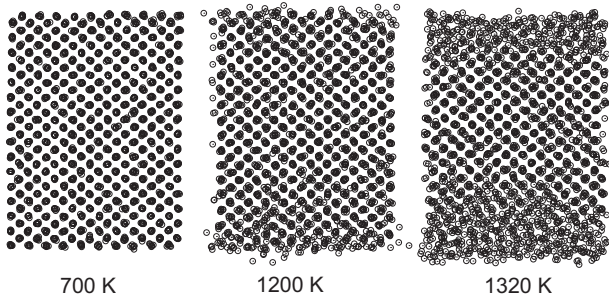


FIG. 3. Typical MC snapshot of the solid film at three temperatures. The open circles mark instantaneous atomic positions projected on the  $(1\bar{1}0)$  plane parallel to the page. Note the perfectly ordered surface structure at low temperatures and premelting at high temperatures.

### E. Thermodynamic integration

The free energy  $\gamma$  of the solid surface was computed as a function of temperature by thermodynamic integration based on Eq. (13).  $U^{\text{ex}}$  was determined from the MC simulations at several temperatures using Eq. (9). The values of  $[U]$  and  $[N]$  were computed for the entire simulation block and  $U^{\text{S}}$  and  $N^{\text{S}}$  for the bulk solid region selected as discussed above. The integrand of Eq. (13) computed at several temperatures was approximated by a fourth-order polynomial and integrated analytically. Increasing the power of the polynomial did not affect the results significantly.

The reference temperature was chosen to be  $T_0=300$  K. The reference value  $\gamma_0$  was obtained in the classical quasi-harmonic approximation to atomic vibrations.<sup>11</sup> It was checked that other choices of  $T_0$  within  $\pm 50$  K produced only minor changes in the results.

## IV. RESULTS

Examination of the MC snapshots shows that the atomically ordered solid surface becomes increasingly disordered at high temperatures, developing a relatively thick liquidlike layer near  $T_m$  (Fig. 3). This trend is quantified in Fig. 4, showing that the surface thickness  $h$  is on the order of the

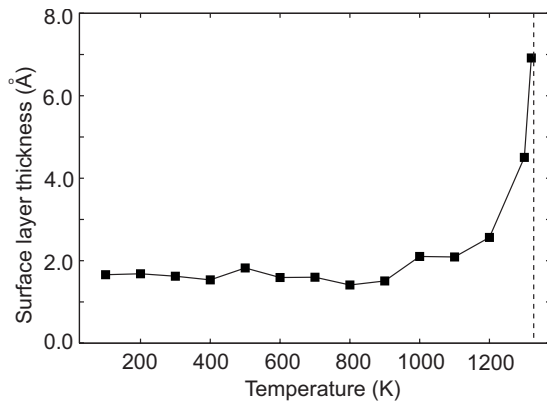


FIG. 4. Thickness of the  $(110)$  surface layer as a function of temperature. The vertical dashed line indicates the bulk melting point.

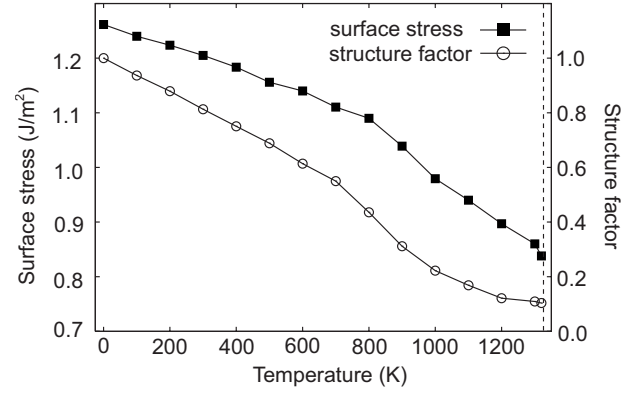


FIG. 5. Average stress  $\tau$  and the surface structure factor  $|S(\mathbf{k})|_{\text{top}}$  of the  $(110)$  surface as a function of temperature. The vertical dashed line indicates the bulk melting point.

interatomic distance at low temperatures but rapidly increases with temperature at  $T > 1100$  K. The thickness appears to diverge to infinity near  $T_m$ , but this remains to be verified by future detailed calculations in a very close vicinity of  $T_m$ . The surface structure factor  $|S(\mathbf{k})|_{\text{top}}$  decreases with temperature approximately linearly until about 800 K (Fig. 5), which can be attributed to increased amplitudes of atomic vibrations in the otherwise atomically perfect surface structure. At temperatures around 800 K, the atoms of the top surface layer begin to abandon their regular positions and jump on top of the layer, forming adatoms and leaving surface vacancies behind. The amount of this structural disorder rapidly increases with temperature. Accordingly,  $|S(\mathbf{k})|_{\text{top}}$  decreases more rapidly than below 800 K, producing a breaking point on the curve. As expected,  $|S(\mathbf{k})|_{\text{top}}$  is small near  $T_m$ , reflecting the formation of a liquidlike layer on the surface.

Because the coordinate axes are chosen to be parallel to crystallographic directions with twofold symmetry, the surface-stress tensor is diagonal. Its components calculated at 0 K using Eq. (6) with  $\sigma_{ij}^s=0$  are  $\tau_{11}=1.19$  J/m<sup>2</sup> and  $\tau_{22}=1.33$  J/m<sup>2</sup>, showing moderate anisotropy. Both components are positive and smaller than the 0 K surface energy,  $\gamma=1.472$  J/m<sup>2</sup>. The average surface stress decreases with temperature from  $\tau=1.26$  J/m<sup>2</sup> at 0 K to 0.83 J/m<sup>2</sup> at 1320 K (Fig. 5). This decrease is almost linear between 0 and about 800 K but accelerates and becomes noticeably nonlinear above 800 K. This behavior is remarkably similar to the temperature dependence of the surface structure factor, demonstrating that  $\tau$  is a sensitive parameter to the surface disordering at high temperatures.

To verify that this similarity is not a numerical artifact arising from the size effect or the simulation method, additional MC calculations of  $\tau$  were conducted for two different block sizes. Furthermore, additional calculations were performed for yet another block size using molecular dynamics instead of MC. The results are summarized in Fig. 6, showing that all the points lie on a common curve whose shape is very similar to Fig. 5.

The anisotropy of the surface stress,  $\tau_{22}-\tau_{11}$ , increases with temperature as long as the surface remains perfectly ordered (Fig. 7), reaches a maximum around 800 K where

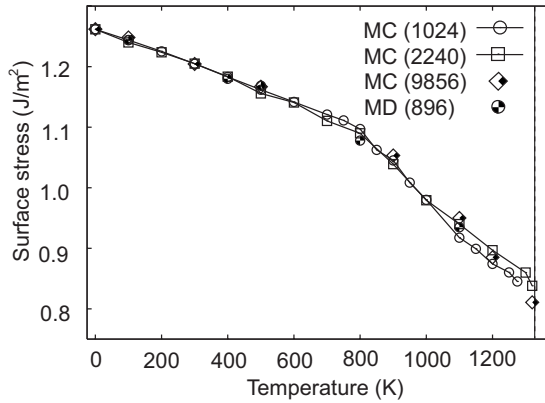


FIG. 6. Temperature dependence of the average surface stress computed by MC simulations of systems with 1024, 2240, and 9856 atoms and by molecular-dynamics simulations of a 896 atom system. Note that the shape of the curve does not depend on the model size or the simulation method.

the surface disordering starts, and then drops and reaches a slightly negative value near the melting point. This behavior confirms the sensitivity of the surface stress to the structural order at the surface, which is consistent with Figs. 5 and 6.

The surface free energy decreases with temperature from  $\gamma=1.472$  J/m<sup>2</sup> at 0 K to 1.130 J/m<sup>2</sup> at 1320 K (Fig. 8), remaining always larger than  $\tau$ . The onset of surface disordering at 800 K is accompanied by a noticeable change in the slope of  $\gamma(T)$  but the curve is much smoother than  $\tau(T)$ . Note that  $\gamma$  and  $\tau$  do not have the same value at the melting point. The liquid-vacuum interface stress at  $T_m$  is  $\tau^l=0.925$  J/m<sup>2</sup>, which can be identified with the free energy  $\gamma^l$  of this interface. This value lies between  $\gamma$  and  $\tau$  for the solid surface.

The solid-liquid interface stress obtained from the solid-liquid coexistence simulations is  $\tau^{sl}=-0.131$  J/m<sup>2</sup>. To give an idea of the error bar, the individual components of the stress are  $\tau_{11}^{sl}=-0.129 \pm 0.035$  J/m<sup>2</sup> and  $\tau_{22}^{sl}=-0.132 \pm 0.033$  J/m<sup>2</sup>. The negative value of the stress indicates that this interface is in a state of compression. This interface stress would produce a biaxial expansion in a free-standing (110) Cu film immersed in its melt at the solid-liquid equilibrium temperature.

Recall that the calculation of  $\tau^{sl}$  included corrections for the residual stresses within the solid. When such corrections

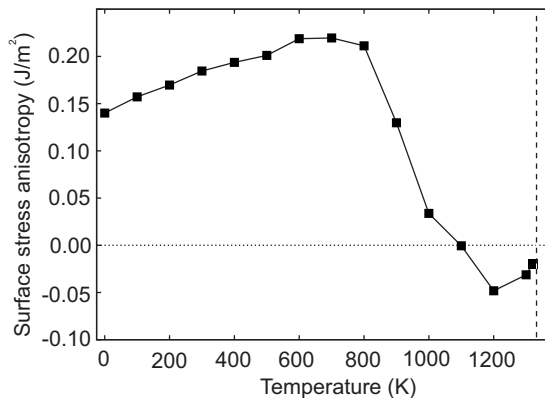


FIG. 7. Temperature dependence of the surface-stress anisotropy  $\tau_{22}-\tau_{11}$ . The vertical dashed line indicates the bulk melting point.

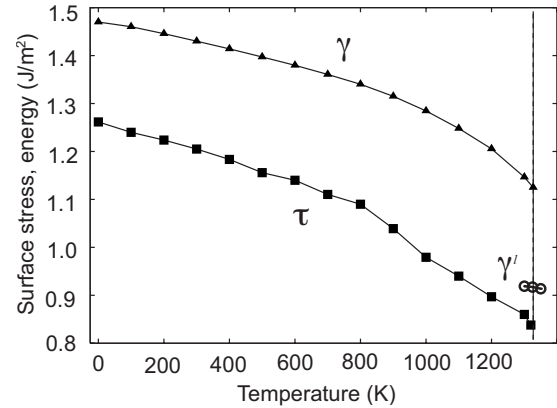


FIG. 8. Temperature dependence of the excess free energy and stress of the (110) surface. Three values of the free energy,  $\gamma^l$ , of the liquid-vacuum interface are shown for comparison. The vertical dashed line indicates the bulk melting point.

were ignored, the interface stress variations during the MC simulations became much larger, resulting in  $\tau_{11}^{sl}=-0.081 \pm 0.177$  J/m<sup>2</sup> and  $\tau_{22}^{sl}=-0.151 \pm 0.175$  J/m<sup>2</sup>. Although the residual stresses were relatively small (on the level of 10 MPa), we see clear indications that taking them into account produces a stabilizing effect and yields more accurate values of the interface stress. The same was found in the surface-stress calculations for the solid and liquid films.

Finally, for the interpretation of the results in Sec. V, we computed the surface stress in the solid film as a function of imposed biaxial strain at 0 K. The strain was increased by small increments from 0 to 0.0252, a range which corresponds to linear thermal-expansion factors at temperatures between 0 and 1320 K. The atomic positions were relaxed after each increment of strain. The surface stress was found to decrease as a linear function of strain from 1.26 J/m<sup>2</sup> at zero strain to 0.941 J/m<sup>2</sup> at the maximum strain.

## V. DISCUSSION AND CONCLUSIONS

We have shown how surface and interface stresses and free energies in elemental systems can be computed as appropriate excesses when the solid phase is in a nonhydrostatic state. Instead of constructing profiles of intensive properties and choosing dividing surfaces,<sup>1</sup> we applied the method of Cahn<sup>4</sup> to express the excess quantities through determinants containing only extensive properties such as the number of atoms, volume, and the total virial stress. All such quantities are immediately accessible by atomistic simulations employing either MC or molecular-dynamics methods. Our approach is general enough to permit extensions to multicomponent systems, solid-solid interfaces, and other complex systems in the future. We applied this method to examine the temperature dependence of the surface free energy and surface stress of (110) copper modeled by an embedded-atom potential. Although thermal expansion was applied to minimize the bulk stress, some residual stress remained and was taken into account in the calculations.

The (110) Cu surface stress was found to decrease with temperature, reaching about 66% of its 0 K value near the

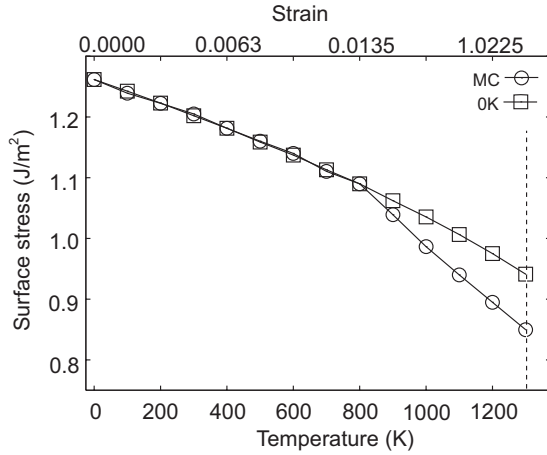


FIG. 9. Temperature and bulk-strain dependencies of the surface stress obtained by MC simulations and by 0 K static calculations. In the latter case, the data are plotted against the temperature at which thermal expansion would give the corresponding strain. The close agreement below 800 K indicates the dominant role of the bond-stretching effect in the temperature dependence of surface stress of atomically ordered surfaces.

bulk melting point. The plot of  $\tau$  versus temperature (Fig. 5) exhibits two distinct parts, which will be discussed separately.

At temperatures from 0 to about 800 K,  $\tau$  decreases with temperature almost linearly. The surface structure remains perfectly ordered (Fig. 3) and the concomitant decrease in the surface structure factor  $|S(\mathbf{k})|_{\text{top}}$  is due to increasing amplitudes of atomic vibrations. The decrease in  $\tau$  could be caused by two physical factors: (i) the vibration factor (the amplitudes at the surface and in the bulk both increase with temperature but at different rates, leading to a change in the excess entropy of the surface) and (ii) the expansion factor (the thermal expansion stretches interatomic bonds, altering the state of tension on the surface). To evaluate the role of the second factor, the  $\tau$  computed as a function of biaxial strain at 0 K is plotted against the temperatures at which the respective strains would be produced by thermal expansion (Fig. 9). The curve is compared with the actual surface stress as a function of temperature. In effect, the two curves represent the surfaces stresses for the same state of lateral strain in the bulk<sup>19</sup> but at different temperatures. The curves are in very close agreement up to 800 K but diverge at higher temperatures. This agreement indicates that as long as the surface structure is perfectly ordered, the decrease in  $\tau$  with temperature is strongly dominated by the bond-stretching effect produced by thermal expansion. This conclusion emphasizes the importance of including thermal-expansion factors in surface-stress calculations at finite temperatures.

At  $T > 800$  K, the surface stress decreases with temperature more rapidly than below 800 K due to rapid accumulation of surface disorder. It is due to this structural disordering that the plots of  $\tau$  and  $|S(\mathbf{k})|_{\text{top}}$  versus temperature have a distinct breaking point at about 800 K.

The surface free energy decreases with temperature (Fig. 8) and is less sensitive to the onset of surface disordering at 800 K. If the strain was kept constant, the slope of  $\gamma$  versus

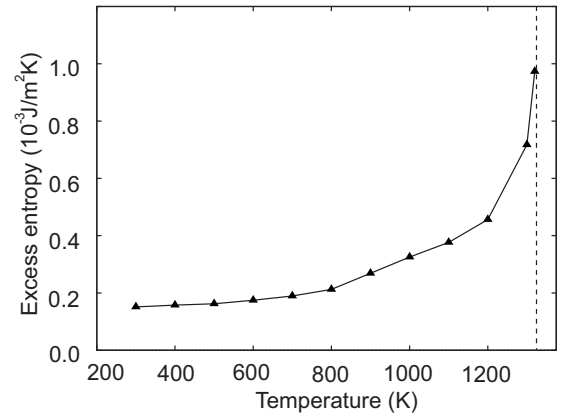


FIG. 10. Temperature dependence of the excess entropy of the (110) Cu surface. The vertical dashed line indicates the bulk melting point.

$T$  would give us the negative of the excess surface entropy. In our simulations, however, the strain was varied with temperature to accommodate the thermal expansion. As a result, our slope includes not only  $S^{\text{ex}}$  but also the work done against the surface stress, which is expressed by the additional term in Eqs. (5) and (11). An omission of this term would be thermodynamically incorrect and, for the particular surface studied here, would underestimate its free energy by about  $0.1 \text{ J/m}^2$  near the melting point. The excess surface entropy  $S^{\text{ex}}$  can be readily determined from Eq. (8) using the obtained values of  $\gamma A$  and  $U^{\text{ex}}$ . This quantity per unit physical area is plotted as a function of temperature in Fig. 10, showing a slow initial growth followed by a rapid acceleration above the surface disordering temperature.

Although the solid surface is covered with a relatively thick (e.g., about  $7 \text{ \AA}$  at 1320 K) liquidlike film at temperatures approaching  $T_m$ , the free energy of the premelted surface remains quite different from the free energy of the liquid-vacuum interface or from the surface stress. This difference can be attributed to the excess quantities associated with the interface between the premelted layer and the bulk solid. As a simple model, the premelted surface can be considered as a layer of real liquid bounded by the solid-liquid and liquid-vacuum interfaces. Neglecting interactions (“disjoining potential”) between these interfaces, the following relations should hold near  $T_m$ :

$$\gamma = \gamma^{sl} + \gamma^l, \quad (22)$$

$$\tau = \tau^{sl} + \gamma^l. \quad (23)$$

In these relations,  $\gamma = 1.130 \text{ J/m}^2$ ,  $\gamma^l = 0.925 \pm 0.018 \text{ J/m}^2$ , and  $\tau = 0.83 \pm 0.012 \text{ J/m}^2$  have been determined by the MC simulations. Solving these equations for  $\gamma^{sl}$  and  $\tau^{sl}$ , we obtain  $\gamma^{sl} = 0.199 \pm 0.018 \text{ J/m}^2$  and  $\tau^{sl} = -0.088 \pm 0.018 \text{ J/m}^2$ . The solid-liquid interface free energy compares well with the experimental value  $\gamma^{sl} = 0.177 \text{ J/m}^2$  from indirect measurements for an average orientation.<sup>20</sup> Likewise, the solid-liquid interface stress deduced from Eq. (23) is in adequate agreement with  $\tau^{sl} = -0.131 \pm 0.034 \text{ J/m}^2$  obtained by the MC simulations.

This consistency indicates that our interpretation of the premelted surface structure as two interfaces is reasonable. We emphasize, however, that this conclusion was reached for the highly energetic (110) surface orientation, which pre-melts more readily than low-energy orientations such as (111). In a separate study, we were able to overheat the (111) Cu surface well above  $T_m$  without the formation of a liquid layer or even significant disordering. The effect of the surface orientation on premelting behavior will be the subject of a separate publication. It is interesting to note that in our simulations of the (110) solid-liquid coexistence, we clearly observed spontaneous formation and destruction of small facets with the (111) orientation. Since this faceting increases the actual interface area, we conclude that the (111) orientation has a lower interface free energy than (110).

Finally, the negative sign of  $\tau^{sl}$  suggests that the (110) solid-liquid interface is in a state of compression, a finding which can have implications for crystal nucleation models. Because this stress is an order of magnitude smaller than typical surface stresses, it is very difficult to measure or compute. Negative values of solid-liquid interface stresses were previously reported for Lennard-Jones<sup>12,21</sup> and hard-sphere<sup>22</sup> systems. It is interesting to note that the hard-sphere simulations gave a larger absolute value of  $\tau^{sl}$  for the (111) orientation than for (100).<sup>22</sup> In a more recent simulation,<sup>13</sup> negative  $\tau^{sl}$  values were obtained for a binary Lennard-Jones system but positive for Ni and Si modeled by embedded-atom and Stillinger-Weber potentials, respectively. Further research into anisotropy of interface stresses is needed to determine whether the negative sign of  $\tau^{sl}$  is a feature of this particular orientation or a general property of copper modeled with this potential.

#### ACKNOWLEDGMENTS

We are grateful to Mark Asta and Brian Laird for stimulating comments on this paper. This work was supported by the Office of Basic Energy Sciences, U.S. Department of Energy. We acknowledge useful discussions facilitated through coordination meetings sponsored by the DOE-BES Computational Materials Science Network (CMSN) program.

#### APPENDIX

In this appendix we present derivations of Eqs. (4) and (14). Consider a rectangular simulation block containing an interface normal to one of its edges  $z$ . The block contains a fixed number of atoms  $N$ , all of which are of the same chemical species, and is subject to periodic boundary conditions in the  $x$  and  $y$  directions parallel to the interface. The  $x$ - $y$  cross section of the solid part of the block contains a fixed number of unit cells. We assume that the solid is in a nonhydrostatic state of stress. It is either exposed to vacuum or in contact and equilibrium with a liquid phase at a pressure  $p$ . The temperature  $T$  is assumed to be homogeneous throughout.

This system can only receive/release heat and do mechanical work by deformation. In such processes, the differential of the total Helmholtz free energy is

$$dF = -SdT + \sum_{i,j=1,2} \sigma_{ij} V de_{ij} + \sigma_{33} A dL, \quad (\text{A1})$$

where  $L$  is the system size in  $z$  and  $\sigma_{ij}$  are the volume-averaged stress components on the lateral faces of the block. The following mechanical equilibrium conditions are assumed to be satisfied everywhere inside the solid: (1)  $\sigma_{33} = -p$  for the solid-liquid interface and  $\sigma_{33} = 0$  for the solid surface, and (2)  $\sigma_{3i} = 0$ ,  $i = 1, 2$ . According to Gibbs' definition of  $\gamma$  as a work term,<sup>1</sup> this quantity can be expressed as the free-energy cost of creating a unit area of new surface/interface in a closed system at a constant  $T$  without doing any other work.

For a solid surface,  $\gamma A$  can be found as the free energy excess over a bulk solid at a constant number of atoms,

$$\gamma A = F - f^s N \equiv [F/N], \quad (\text{A2})$$

where  $f^s$  is the free energy per atom of the homogeneous solid phase. Taking a differential of Eq. (A2) at constant  $N$  and combining it with  $dF$  from Eq. (A1),

$$d(\gamma A) = -SdT - Ndf^s + \sum_{i,j=1,2} \sigma_{ij} V de_{ij}. \quad (\text{A3})$$

Applying the same procedure to Eq. (A2) with  $\gamma A = 0$ , we obtain the Gibbs-Duhem equation for the bulk solid,

$$0 = -S^s dT - N^s df^s + \sum_{i,j=1,2} \sigma_{ij}^s V^s de_{ij}. \quad (\text{A4})$$

The system of two equations, Eqs. (A3) and (A4), can be solved for  $d(\gamma A)$  using Cramer's rule,<sup>4</sup>

$$d(\gamma A) = -[S/X]dT - [N/X]df^s + \sum_{i,j=1,2} [\sigma_{ij} V/X] de_{ij}, \quad (\text{A5})$$

which is identical to Eq. (4) of the main text. Depending on the choice of  $X$ , one of the terms in Eq. (A5) vanishes and the corresponding variable becomes a function of the remaining independent variables.

For the solid-liquid interface, since the interface creation can be accompanied by a volume effect, the corresponding mechanical work (if  $p \neq 0$ ) must be eliminated by identifying  $\gamma A$  with the excess of  $F$  at constant  $N$  and  $V$ ,

$$\gamma A = [F/NV] = \frac{\begin{vmatrix} F & N & V \\ F^s & N^s & V^s \\ F^l & N^l & V^l \end{vmatrix}}{\begin{vmatrix} N^s & V^s \\ N^l & V^l \end{vmatrix}}. \quad (\text{A6})$$

The free energies of the bulk phases are given by

$$F^l = -pV^l + N^l \mu, \quad (\text{A7})$$

$$F^s = -pV^s + N^s \mu, \quad (\text{A8})$$

where  $\mu$  is the chemical potential in the liquid. (Note that these equations include only the liquid chemical potential; see Gibbs' discussion of the nonuniqueness of chemical potential of nonhydrostatic solids.<sup>1</sup>) Equation (A8) expresses

the solid-liquid equilibrium condition derived by Gibbs.<sup>1</sup> Substituting Eqs. (A7) and (A8) in Eq. (A6), it is straightforward to obtain

$$\gamma A = F - \mu N + pV. \quad (\text{A9})$$

Taking a differential of Eq. (A9) at constant  $N$  and using Eq. (A1) in conjunction with  $dV = V \sum_{i,j=1,2} \delta_{ij} de_{ij} + AdL$ , we arrive at

$$d(\gamma A) = -SdT + Vdp - Nd\mu + \sum_{i,j=1,2} (\sigma_{ij} + \delta_{ij}p) V de_{ij}. \quad (\text{A10})$$

This equation should be considered simultaneously with the Gibbs-Duhem equations for the bulk phases, which are easily obtained from Eq. (A10) by setting  $\gamma A \equiv 0$ ,

$$0 = -S^s dT + V^s dp - N^s d\mu + \sum_{i,j=1,2} (\sigma_{ij}^s + \delta_{ij}p) V^s de_{ij}. \quad (\text{A11})$$

$$0 = -S^l dT + V^l dp - N^l d\mu. \quad (\text{A12})$$

Using these bulk equations, any two terms in Eq. (A10) can be eliminated by applying Cramer's rule,<sup>4</sup>

$$d(\gamma A) = -[S/XY]dT + [V/XY]dp - [N/XY]d\mu + \sum_{i,j=1,2} [(\sigma_{ij} + \delta_{ij}p)V/XY]de_{ij}, \quad (\text{A13})$$

where the notation  $[Z/XY]$  is explained by Eq. (15).

The above equations include the extensive quantities  $S$ ,  $V$ ,  $N$ , and  $\sigma_{ij}V$  related to the entire simulation block. However, their excesses do not change if, instead of the entire block, we use a narrower layer containing the surface/interface. As long as the bounds of the layer are beyond the influence of the surface/interface, the addition of new bulk regions results only in adding multiples of the second and/or third rows of the determinants to the first one, which does not change the value of the determinant.<sup>4</sup> Designating the layer properties by square brackets, Eqs. (A5) and (A13) become completely equivalent to Eqs. (4) and (14) appearing in the main text.

\*tfrolov@gmu.edu

†ymishin@gmu.edu

<sup>1</sup>J. W. Gibbs, *The Collected Works of J. W. Gibbs* (Yale University Press, New Haven, 1948), Vol. 1.

<sup>2</sup>R. Shuttleworth, Proc. Phys. Soc., London, Sect. A **63**, 444 (1949).

<sup>3</sup>D. Kramer and J. Weissmuller, Surf. Sci. **601**, 3042 (2007).

<sup>4</sup>J. W. Cahn, in *Interface Segregation*, edited by W. C. Johnson and J. M. Blackely (American Society for Metals, Metals Park, OH, 1979), Chap. 1, p. 3.

<sup>5</sup>R. C. Cammarata, Prog. Surf. Sci. **46**, 1 (1994).

<sup>6</sup>J. W. M. Frenken, P. M. J. Maree, and J. F. van der Veen, Phys. Rev. B **34**, 7506 (1986).

<sup>7</sup>C. Gurney, Proc. Phys. Soc., London, Sect. A **62**, 639 (1949).

<sup>8</sup>G. L. J. Bailey and H. Watkins, Proc. Phys. Soc., London, Sect. A **63**, 350 (1949).

<sup>9</sup>C. Herring, in *Structure and Properties of Solid Surfaces*, edited by R. Gomer and C. S. Smith (University of Chicago Press, Chicago, 1953), Chap. 1, pp. 5-81.

<sup>10</sup>J. S. Vermaak and D. K. Wilsdorf, J. Phys. Chem. **72**, 4150 (1968).

<sup>11</sup>S. M. Foiles, Phys. Rev. B **49**, 14930 (1994).

<sup>12</sup>J. Q. Broughton and G. H. Gilmer, Acta Metall. **31**, 845 (1983).

<sup>13</sup>C. A. Becker, J. J. Hoyt, D. Buta, and M. Asta, Phys. Rev. E **75**, 061610 (2007).

<sup>14</sup>J. W. Cahn, Acta Metall. **28**, 1333 (1980).

<sup>15</sup>Y. Mishin, M. J. Mehl, D. A. Papaconstantopoulos, A. F. Voter, and J. D. Kress, Phys. Rev. B **63**, 224106 (2001).

<sup>16</sup>S. M. Foiles, Phys. Rev. B **32**, 7685 (1985).

<sup>17</sup>S. M. Foiles, in *Surface Segregation Phenomena*, edited by P. Dowben and A. Miller (CRC, Boca Raton, FL, 1990), p. 79.

<sup>18</sup>P. Gumbsch and M. S. Daw, Phys. Rev. B **44**, 3934 (1991).

<sup>19</sup>Note that the normal strains in the bulk are different; the thermal expansion in the normal direction is not captured by the 0 K calculations.

<sup>20</sup>L. E. Murr, *Interfacial Phenomena in Metals and Alloys* (Addison-Wesley, Reading, MA, 1975).

<sup>21</sup>J. Q. Broughton and G. H. Gilmer, J. Chem. Phys. **84**, 5759 (1986).

<sup>22</sup>R. L. Davidchack and B. B. Laird, J. Chem. Phys. **108**, 9452 (1998).